HAL
open science

Numerical study of heat transfer in square millimetric zigzag channels in the laminar flow regime

Hanbin Shi, Nathalie Di Miceli Raimondi, David F. Fletcher, Michel Cabassud, Christophe Gourdon

To cite this version:

Hanbin Shi, Nathalie Di Miceli Raimondi, David F. Fletcher, Michel Cabassud, Christophe Gourdon. Numerical study of heat transfer in square millimetric zigzag channels in the laminar flow regime. Chemical Engineering and Processing: Process Intensification, 2019, 144, pp.0. 10.1016/j.cep.2019.107624 . hal-02345630

HAL Id: hal-02345630

https://hal.science/hal-02345630v1

Submitted on 4 Nov 2019

HAL is a multi-disciplinary open access archive for the deposit and dissemination of scientific research documents, whether they are published or not. The documents may come from teaching and research institutions in France or abroad, or from public or private research centers.

L'archive ouverte pluridisciplinaire **HAL**, est destinée au dépôt et à la diffusion de documents scientifiques de niveau recherche, publiés ou non, émanant des établissements d'enseignement et de recherche français ou étrangers, des laboratoires publics ou privés.

Open Archive Toulouse Archive Ouverte

OATAO is an open access repository that collects the work of Toulouse researchers and makes it freely available over the web where possible

This is an author's version published in: http://oatao.univ-toulouse.fr/24331

Official URL: https://doi.org/10.1016/j.cep.2019.107624

To cite this version:

Shi, Hanbin and Di Miceli Raimondi, Nathalie and Fletcher, David F. and Cabassud, Michel and Gourdon, Christophe *Numerical study of heat transfer in square millimetric zigzag channels in the laminar flow regime.* (2019) Chemical Engineering and Processing: Process Intensification, 144. ISSN 0255-2701

Any correspondence concerning this service should be sent to the repository administrator: tech-oatao@listes-diff.inp-toulouse.fr

Numerical study of heat transfer in square millimetric zigzag channels in the laminar flow regime

Hanbin Shi[a], Nathalie Di Miceli Raimondi[a,*], David F. Fletcher[b], Michel Cabassud[a], Christophe Gourdon[a]

[a] Laboratoire de Génie Chimique, Université de Toulouse, CNRS, INPT, UPS, Toulouse, France
[b] School of Chemical and Biomolecular Engineering, The University of Sydney, NSW, 2006, Australia

A B S T R A C T

The present work deals with the simulation of heat transfer in zigzag millimetric channels with square cross-section of 2 mm width in the laminar flow regime. They consist of periodic zigzag units composed of straight sections and 90° bends with a curvature radius of 1.5 mm. The influences of fluid velocity and straight section length on the thermo-hydraulic performances are investigated. The results showed that by increasing the flow velocity or decreasing the straight section length between two bends, a transition from periodic flow to non-periodic flow can be observed. A thermo-hydraulic performance factor based on heat transfer enhancement and pressure drop penalty compared with a straight channel is then discussed. It is observed that the ratio of the Nusselt number in the zigzag channels to that in the straight channel is always higher than one. This ratio increases with increasing Reynolds number and values up to 6.4 are reached in the cases studied (Pr = 6.13). When the pressure drop penalty is considered in the performance factor, an enhancement is still observed with a factor up to 2.5. It is shown that non-periodic flow is not particularly interesting in terms of thermo-hydraulic performance compared with periodic flow.

1. Introduction

In the process intensification field, new technologies like compact heat exchangers-reactors have been developed over the past decade to meet the trend of safer, cleaner, more effective and less energy-consuming processes. They integrate two basic concepts of process intensification which are on one hand the miniaturization of the units and on the other hand the multi-functionalization of the apparatuses, exhibiting many advantages, such as good heat transfer performances, better temperature control and reactive volume confinement. Anxionnaz et al. [1] made a review of different kinds of compact heat exchangers-reactors and presented their applications at pilot scale or industrial scale. However, the reactor size reduction results in laminar flow operating conditions which does not favour transport phenomena. Consequently, complex designs are required in order to enhance mass and heat transfer. Wavy geometries are often applied in compact heat exchangers reactors since many techniques are today available and effective to design such geometries in various materials, such as metals or silicon carbide with good accuracy and low wall roughness. Moreover they offer good heat exchange performances as they can decrease the thermal boundary layer thickness compared with straight tubes [2].

In order to explain the significant global enhancement of heat transfer in wavy channels compared with straight channels in laminar flow, many studies have been conducted to understand the relationship between hydrodynamics in wavy channels and heat transfer coefficients. The secondary flow (Dean vortices) generated in curved passages is the main effect for the improvement of mixing and heat transfer. Manglik et al. [3] studied numerically the steady forced convection in wavy plate-fin channels at low Reynolds number and found the generation of secondary flow which enhanced the heat transfer as well as the pressure drop penalty. Wang and Liu [4] presented various secondary flow structures in slightly curved microchannels with square cross-section. Their results suggested that the secondary flow created by channel curvature can increase the Nusselt number significantly and the friction factor moderately. Sui et al. [5,6] performed numerical and experimental studies of heat transfer for laminar liquid-water flow in three-dimensional wavy microchannels with rectangular cross- section. Their results also showed that the heat transfer performance in wavy microchannels was much better than that of straight microchannels with the same cross-section due to the generation of secondary flow and that the pressure drop penalty could be much smaller that the heat transfer enhancement. Fletcher and his coworkers [7–13] have

* Corresponding author.
E-mail address: nathalie.raimondi@iut-tlse3.fr (N. Di Miceli Raimondi).

https://doi.org/10.1016/j.cep.2019.107624

Nomenclature

A	cross-sectional area (m^2)
A_H	heat exchange area (m^2)
C_p	specific heat of the fluid (J kg^{-1} K^{-1})
da	element of cross-sectional area (m^2)
d_h	hydraulic diameter (m)
dl	element of perimeter length (m)
dX	element of development length (m)
e	thickness of aluminum plate (m)
e_h	heat transfer enhancement factor
f	local Fanning friction factor
f_i	frequency i (Hz)
h	heat transfer coefficient (W m^{-2} K^{-1})
H	enthalpy (J kg^{-1})
L	channel length (m)
L_c	curved section length (m)
L_s	straight section length (m)
$\dot{m}$	mass flow rate (kg s^{-1})
$\boldsymbol{n}$	normal vector at a cross-section
N_{bend}	number of bends
N_c	number of divisions along the curved section
N_d	number of divisions for the channel depth and width
N_e	number of computational volume elements
N_s	number of divisions along the straight section
N_{unit}	number of periodic units
Nu	local Nusselt number
p	pressure (Pa)
$\bar{p}$	area average pressure (Pa)
Δp	pressure drop (Pa)
P	cross-section perimeter length (m)
$\mathscr{P}$	flow friction power (W)
PF	performance factor
Pr	Prandtl number
q	heat flux (W)
q_l	thermal loss (W)
Q	volumetric flowrate (m^3 s^{-1})
R_c	radius of curvature (m)
Re	Reynolds number
T	temperature (K)
$\bar{T}$	area average temperature (K)
$\bar{T}_b$	bulk temperature (K)
$\bar{T}_w$	peripheral average temperature at the wall (K)
ΔT_{ml}	logarithmic mean temperature difference (K)
$\boldsymbol{u}$	velocity vector (m s^{-1})
$\bar{u}$	mean fluid velocity (m s^{-1})
U	global heat transfer coefficient (W m^{-2} K^{-1})
x	coordinate over the developed length (m)
y	coordinate over the channel width (m)
z	coordinate over the channel depth (m)

Greek symbols

θ	angle between two straight sections (°)
λ	thermal conductivity (W m^{-1} K^{-1})
μ	dynamic viscosity (Pa s)
ρ	fluid density (kg m^{-3})
σ_T	standard temperature deviation (K)

Subscripts

0	value in straight channel
m	mean value over channel length
p	process fluid
u	utility fluid
w	wall
x	relative to axial location x

Superscripts

∞	hydrodynamically and thermally fully-developed flow

conducted a variety of numerical studies for steady laminar flow and heat transfer in zigzag channels with different cross-sections and different unit paths, including trapezoidal, serpentine, and sinusoidal channels. They found the similar conclusion that Dean vortices can enhance heat transfer greatly with relatively small pressure drop penalty. In addition to Dean vortices, mixing and heat transfer in a wavy passage can be enhanced by chaotic advection, which was described by Aref [14]. This flow behavior can be achieved in two-dimensional unsteady flow or in three-dimensional laminar steady flow. Liu et al. [15] presented a three-dimensional serpentine microchannel design as a way to implement chaotic advection to improve fluid mixing. Stroock et al. [16] and Aubin et al. [17] presented another passive method based on staggered herringbone mixer to generate chaotic flow to mix streams in microchannels at low Reynolds number. Jiang et al. [18] investigated mixing in curved microchannels numerically and experimentally. Their results showed that axial dispersion was substantially reduced relative to a straight channel due to mass transfer enhancement originating from the chaotic flow. Kumar and Nigam [19] studied the heat transfer numerically in a chaotic configuration of circular cross-section in the laminar regime. Their results showed a 25–36% enhancement in the heat transfer coefficient due to chaotic mixing while relative pressure drop was increased by 5–6%. Castelain et al. [20,21] have conducted experimental studies of chaotic advection in a twisted duct with square cross-section. They characterized the chaotic flow and found that it was sensitive to the initial conditions. A coiled heat exchanger based on chaotic advection was designed and it showed 15–18% higher efficiency than a helically coiled tube heat exchanger. Acharya et al. [22] studied numerically and experimentally the heat transfer in an alternating axis coil, their results showed 6–8% higher in-tube heat transfer coefficient due to chaotic mixing compared with a conventional constant axis coil, with a pressure drop increase of 1.5–2.5%.

Adequate criteria should be used to attest of the efficiency of heat exchanger designs as described by Zheng et al. for heat exchangers with various enhanced surfaces [23]. Pati et al. [24] studied the heat transfer performances of two wavy channels: a raccoon channel and a serpentine channel. By comparing average Nusselt number as a function of Reynolds number, the raccoon channel appeared to perform better. However, by using a criterion that integrates both Nusselt number and pressure drop, the serpentine design can be considered as more efficient. This criterion defined as a thermo-hydraulic performance factor PF is very useful to compare heat transfer technologies (Eq. (1)). This factor considers a straight tube as the reference. It is expressed as the ratio of the heat exchange capacity (global heat transfer coefficient h_m multiplied by heat exchange area A_H) in the considered technology to that in a straight tube divided by the ratio of the flow friction power in the technology $\mathscr{P}$ to that in a straight tube $\mathscr{P}_0$:

$$PF = \frac{(h_m A_H / h_0 A_{H,0})}{(\mathscr{P}/\mathscr{P}_0)} \tag{1}$$

The flow friction power depends on the pressure drop Δp in the channel and the volumetric flowrate Q:

$$\mathscr{P} = \Delta p \bullet Q \tag{2}$$

In the present work, a numerical method is developed to study the

flow and heat transfer in a zigzag millimetric channel with square cross-sections under laminar flow regime. The geometry of the channel, presented in Fig. 1, consists of periodic zigzag units. The geometric parameters are the width of the square section d_h (equal to the hydraulic diameter), the radius of curvature of the bends R_c, the length of the straight section L_s and the angle between two straight sections θ. This pattern has been used to build compact heat exchangers-reactors designed by the Laboratoire de Génie Chimique (LGC, France), Boostec (French company) and the Commissariat à l'Energie Atomique et aux Energies Alternatives (CEA, France). Such devices ($d_H = 2$ mm, $R_c = 1.5$ mm, $\theta = 90°$ and $L_s = 7$ mm) made of silicon carbide or stainless steel have been successfully used to carry out highly exothermic reactions [25–27]. The straight channel with the same cross-section as the wavy channel is also studied as a reference.

The impacts of fluid velocity and channel geometry, in terms of straight section length between two bends, on the thermo-hydraulic performances are investigated. The objective is to examine how the residence time of the fluid in the curved section compared with that in the straight section affects the thermo-hydraulic performances. To our knowledge, such a study has not been carried out with square millimetric zigzag channel. Heat transfer coefficients and friction factors are deduced from temperature and pressure fields and compared with those obtained in a straight channel. Fourier analysis is used to detect the onset of non-periodic flow as a function of Reynolds number and straight length between two bends. This method is very often used to describe flow transition by studying the evolution of local velocity components [28–32]. In the present work, it has been applied in an original way to the local Nusselt number and friction factor profiles along the channel. The heat transfer enhancement is then quantitatively reported. The results are finally discussed in terms of a performance factor that takes into account the pressure drop penalty considering that a zigzag channel and a straight channel of same cross-section should offer the same heat exchange capacity and heat or cool the same fluid flowrate.

2. Numerical method

2.1. Equations and solution method

The simulation work is based on the resolution of the equations for the conservation of mass, momentum and energy. For an incompressible fluid and a steady state, these equations can be written as follows:

Continuity equation:

$$\nabla \cdot (\rho \boldsymbol{u}) = 0 \tag{3}$$

Momentum equation (Navier-Stokes):

$$\nabla \cdot (\rho \boldsymbol{u} \otimes \boldsymbol{u}) = -\nabla p + \nabla \cdot (\mu (\nabla \boldsymbol{u} + \nabla \boldsymbol{u}^T)) \tag{4}$$

Energy equation:

$$\nabla \cdot (\rho \boldsymbol{u} H) = \nabla \cdot (\lambda \nabla T) \tag{5}$$

$\boldsymbol{u}$ is the velocity vector, p the pressure, H the enthalpy and T the temperature. The fluid physicochemical properties, such as density ρ, dynamic viscosity μ and thermal conductivity λ, are assumed to be constant (at 25 °C), which make the Prandtl number constant as well ($Pr = 6.13$). No phase change is considered. At the inlet, the fluid temperature is constant (equal to 20 °C) and fully-developed flow is assumed. The Poiseuille velocity profile at the inlet is approximated using the expressions suggested by Shah and London [33]. At the outlet, zero static gauge pressure is set. At the walls, the no-slip condition and constant heat flux (H2) boundary condition are applied.

Table 1
Numbers of bends and units in the zigzag channels with different straight section lengths.

Geometry	'a'	'b'	'c'	'd'	'e'	'f'	'g'
L_s (mm)	2	3.5	4.5	5.5	7	9	12
N_{bend}	22	16	14	12	10	8	6
N_{unit}	11	8	7	6	5	4	3
L/(m)	0.096	0.094	0.096	0.094	0.094	0.091	0.086

The simulations were carried out by solving the system of equations with the finite volume CFD code ANSYS CFX 16. All the calculations were performed at steady state in the laminar flow regime. The convective terms were discretized using a second-order bounded differencing scheme. The system was deemed to having reached a converged state when all the locally-scaled residuals fell below 10^{-6}.

2.2. Computational domain and meshing method

For all the geometries studied, the computational domain consists of a three-dimensional zigzag channel of total length equal to roughly 0.1 m. Depending on the straight section length L_s, the number of bends varies from one geometry to another (in total 7 geometries). Table 1 summarizes the number of bends N_{bend} and units N_{unit} for each case. A unit consists of two straight sections and two bends (Fig. 2(b)). All the geometries start and end with a straight section. However, to avoid the potential effects near the outlet which may influence the results, the last straight section is not taken into account in post-processing calculations. Therefore the total length of the channel L considered in the rest of the article corresponds to a number of entire units.

A swept hexahedral mesh is used for the computational domain to provide an efficient and accurate resolution. In the cross-section, the mesh was constructed to be finer near the wall than at the centre, as shown in Fig. 2(a), since the fluid velocity and temperature gradients are much higher there. Along the axial direction, the mesh was constructed to be uniform, as shown in Fig. 2(b). A mesh is defined by three numbers of divisions:

- along the channel depth and width, N_d, corresponding to a discretized length equal to d_h;
- along the straight section, N_s, corresponding to a discretized length equal to L_s;
- along the curved section in the bend, N_c, corresponding to a discretized length in the center of the channel equal to L_c.

3. Results and discussion

3.1. Parameters of interest: definitions

From the computed velocity, pressure and temperature fields, parameters of interest are calculated during post-processing. A coordinate reference that follows the main direction of the fluid is used. x is the axial coordinate, normal to the cross-section. At the channel inlet, $x = 0$; at the channel outlet, $x = L$. y and z are the coordinates along the channel width and depth, respectively. By convention, a bar above a parameter refers to an area or peripheral average value. The subscript m is used to refer to a mean value over the axial length. A represents the

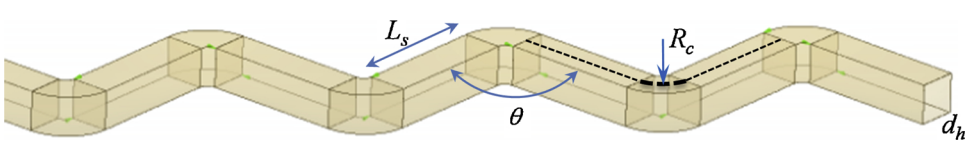

Fig. 1. Schematic of the zigzag channel: $d_h = 2$ mm, $L_s = 2$–12 mm, $R_c = 1.5$ mm, $\theta = 90°$.

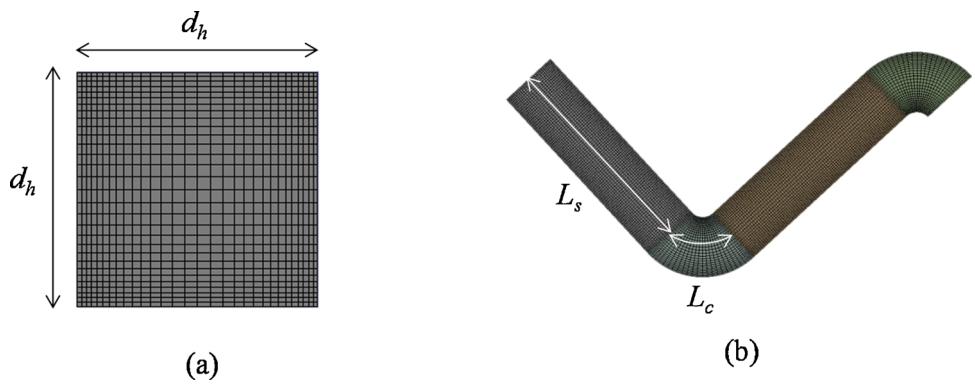

Fig. 2. Illustration of the mesh for one repeating unit on (a) the cross-section and (b) the wall. d_h = 2 mm, L_s = 2–12 mm, L_c = 2.4 mm.

cross-sectional area of the channel and P the cross-section perimeter length. The heat transfer coefficient at axial location x is defined as:

$$h(x) = \frac{q_w}{\bar{T}_w(x) - \bar{T}_b(x)} \tag{6}$$

where q_w is the wall heat flux, $\bar{T}_w$ is the peripheral mean wall temperature and $\bar{T}_b$ is the bulk fluid temperature. The peripheral mean wall temperature is calculated as:

$$\bar{T}_w(x) = \frac{1}{P}\int_{P_x} T_w \, dl \tag{7}$$

where P_x refers to the cross-section perimeter at axial location x. The bulk fluid temperature is calculated using Eq. (8). A_x refers to the cross-sectional area at axial location x. $\boldsymbol{n}$ is the normal vector of the cross-section towards the main direction of the flow.

$$\bar{T}_b(x) = \frac{1}{A\bar{u}}\int_{A_x} (\boldsymbol{u}\cdot\boldsymbol{n}) T \, da \tag{8}$$

The local Nusselt number Nu is defined as:

$$Nu(x) = \frac{h(x) d_h}{\lambda} \tag{9}$$

The average Nusselt number Nu_m between inlet and axial location x is defined as:

$$Nu_m(x) = \frac{1}{x}\int_0^x Nu \, dX \tag{10}$$

The local Fanning friction factor f is defined as:

$$f(x) = -\frac{1}{2}\frac{d_h}{\rho \bar{u}^2}\frac{d\bar{p}}{dX}\bigg|_{X=x} \tag{11}$$

where $\bar{u}$ is the mean fluid velocity, constant along the channel, and $\bar{p}$ is the cross-sectional area average pressure, calculated by:

$$\bar{p}(x) = \frac{1}{A}\int_{A_x} p \, da \tag{12}$$

The average Fanning friction factor f_m between inlet and axial location x is defined as:

$$f_m(x) = \frac{1}{x}\int_0^x f \, dX \tag{13}$$

The results will be discussed in terms of the Reynolds number Re defined as follows:

$$Re = \frac{\rho d_h \bar{u}}{\mu} \tag{14}$$

3.2. Grid independence studies

Grid independence studies were carried out to make sure that the size of the grid did not influence the resulting solution for all the simulations carried out. The local Nusselt number Nu and local Fanning friction factor f were assessed for different mesh densities. Grid independence studies for geometry 'f' at Re = 560 and geometry 'b' at Re = 224 are presented. The variation of the local Nusselt number for different meshes, whose characteristics are given in Table 2, is shown in Fig. 3. For geometry 'f' at Re = 560, from mesh (2) to mesh (3), the local Nusselt number hardly varies and the global average Nusselt number (Nu_m) varies by only 0.35%. Therefore mesh (2) is adequate for this case study with 7.6 million volume elements (N_e) in the computational domain. For geometry 'b' at Re = 224, N_{um} varies by 0.54% while N_e is significantly increased. These two cases have been considered to illustrate the grid independence study because they present two different level of complexity in terms of local thermal behaviors as can be seen in Fig. 3. This will be discussed further in section 3.3.2.

3.3. Local results

3.3.1. Analysis of the temperature field

As expected, it is observed that the temperature field over a cross-section in the zigzag channel is more homogeneous than in the straight channel. For example, Fig. 4(a) and (b) show the temperature field in the straight channel and in the zigzag channel 'e', respectively, at x = 0.075 m (outlet of the 8th bend in the zigzag channel) for Re = 224. In the straight channel, characterized by a laminar Poiseuille flow (Fig. 4(c)), the heating of the successive concentric flow layers occurs by thermal diffusion. In the zigzag channel, the Dean vortices generated by the bends (Fig. 4(d)) create radial mixing which improves the temperature homogenization over the channel cross-section.

For further comparison, the value of the relative maximum temperature difference (T_{max} - T_{min})/ $\bar{T}$ and the relative standard temperature deviation σ_T/ $\bar{T}$ (Eq. (15)) over the cross-section at x = 0.075 m for both channels are calculated at different Reynolds numbers and shown in Fig. 5.

$$\frac{\sigma_T}{\bar{T}} = \frac{\sqrt{\frac{1}{A}\int_{A_x}(T-\bar{T})^2 da}}{\bar{T}} \tag{15}$$

Table 2
Characteristics of the meshes used for geometry 'f' at Re = 560.

	Geometry 'f' (L_s = 12 mm) Re = 560			Geometry 'b' (L_s = 3.5 mm) Re = 224	
Mesh	(1)	(2)	(3)	(1)	(2)
N_d	40	60	80	40	60
N_s	120	180	240	120	180
N_c	40	60	80	40	60
N_e (million)	2.2	7.6	18	4.3	14.5
Nu_m	20.19	19.84	19.77	20.19	19.84

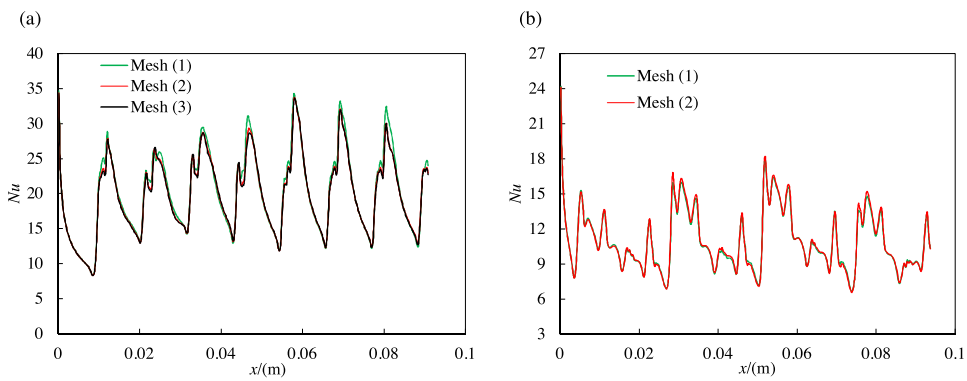

Fig. 3. Mesh influence on the local Nusselt number in (a) geometry 'f' for Re = 560 and (b) geometry 'b' for Re = 224.

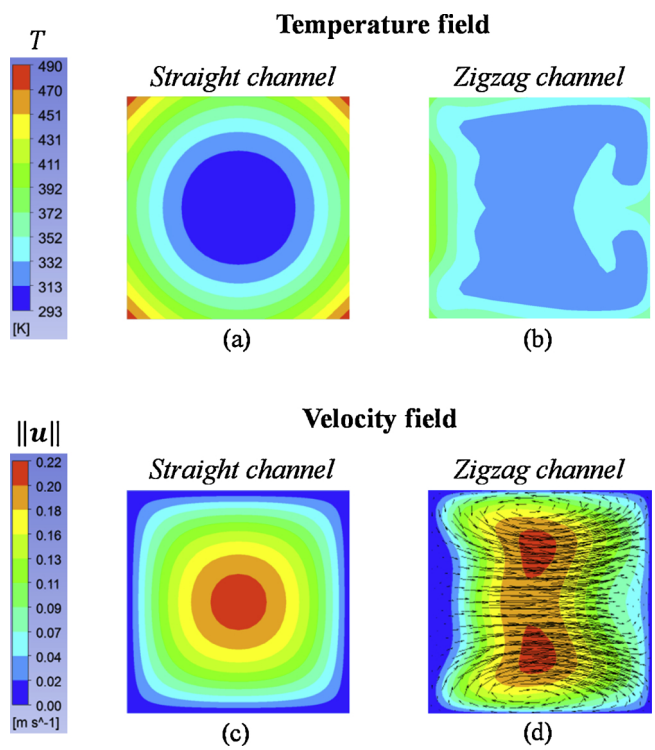

Fig. 4. Temperature and velocity fields over the cross-section at x = 0.075 m in (a, c) the straight channel and in (b, d) the zigzag channel 'e' for Re = 224. The black arrow is the tangential velocity.

$(T_{max} - T_{min})/\bar{T}$ and σ_T decrease both in the zigzag channel and the straight channel with increasing Reynolds number. $(T_{max} - T_{min})/\bar{T}$ and $\sigma_T/\bar{T}$ in the zigzag channel are significantly smaller than in the straight channel, indicating the temperature in the zigzag channel is more homogeneous as mentioned previously. For the design of compact heat exchangers-reactors, this is very favorable when exo- or endothermic reactions are carried out since it avoids extreme temperatures and therefore leads to better control of reactant conversion, limits the formation of by-products and the device operates under safer conditions.

3.3.2. Evolution of Nu and f versus Re

The results obtained in the zigzag channel 'e' are used to illustrate the flow and heat transfer and are compared with the results for the straight channel. The local Nusselt number Nu and Fanning friction factor f from the channel entrance to the exit of the 5th unit in the zigzag channel for Re = 112–448 are shown in Fig. 6. The profiles in the straight channel are also presented. In the straight channel, the local Nusselt number decreases along the channel (Fig. 6(a–d)). This is typical of the thermal boundary layer development in laminar flow as a constant fluid temperature has been set at the channel inlet in the simulations. The asymptotic value of Nu obtained in the simulations at high x is consistent with the theory. Indeed Nusselt number of 3.091 should be reached for hydrodynamically and thermally fully-developed laminar flow in the case of square channels with (H2) thermal boundary condition for all Re [34]. The local Fanning friction factor in the straight channel is constant since a fully-developed laminar flow has been set at the channel entrance (Fig. 6(e–h)). The slight increase observed in the very first millimeters is due to the approximate laminar velocity profiles set at the inlet. The values of f fit with the theory that gives $f = (14.227/Re)$ for fully- developed laminar flow [34].

In the zigzag channel, the evolution of Nu and f in the entrance zone perfectly fits with those observed in the straight channel as the zigzag channel starts with a straight section. Then, oscillations appear that correspond to the periodicity of the geometry studied. Both Nu and f start to increase just before the bends and decrease in the straight section lengths. It can be observed that Nu and f in the zigzag channel are significantly higher globally than those in the straight channel,

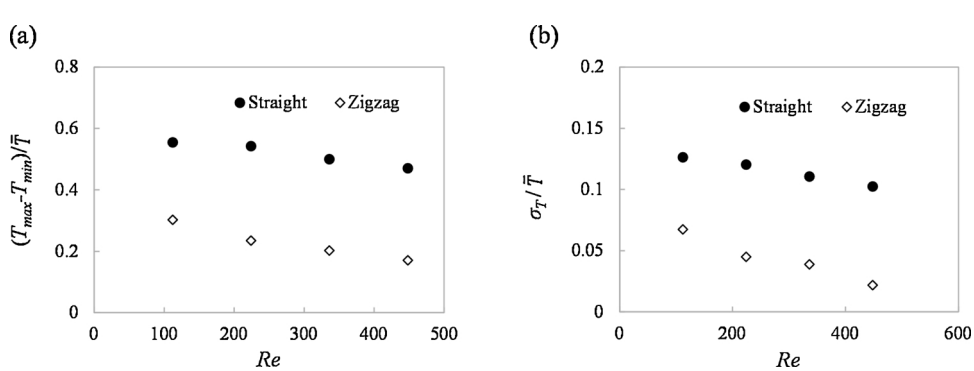

Fig. 5. (a) Relative maximum temperature difference and (b) relative standard temperature deviation over the cross-section at x = 0.075 m in the straight channel and the zigzag channel 'e' versus Reynolds number.

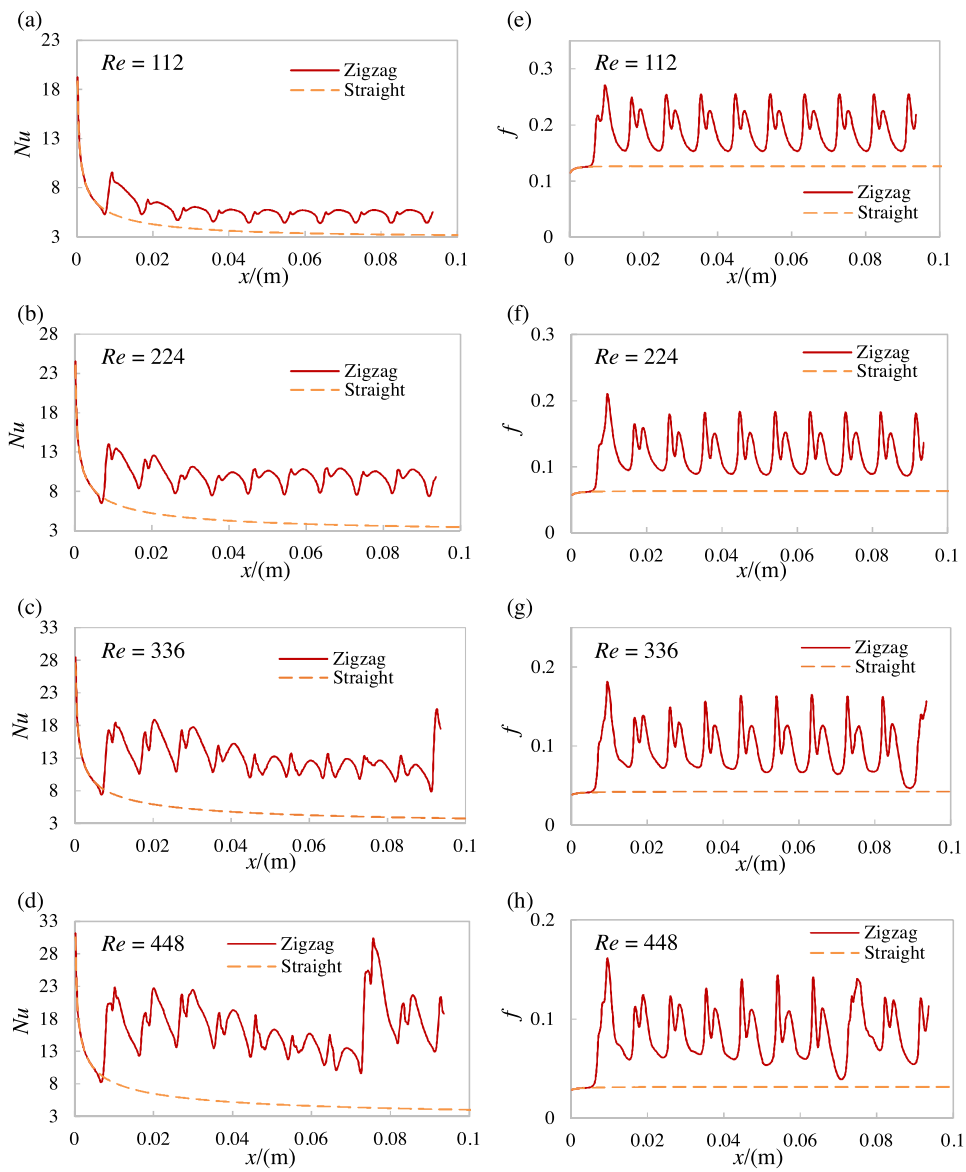

Fig. 6. (a–d) Local Nusselt number and (e–h) Fanning friction factor profiles in the straight channel and zigzag channel 'e' for Re = 112–448.

suggesting as expected that the bends enhance heat transfer but cause additional pressure loss. Nu increases with Re in the zigzag channel, while it is roughly constant in the straight channel. For both channel configurations, f decreases as Re increases. In the zigzag channel it is particularly observable that the oscillations in Nu and f are regular at low Reynolds number from the 4th bend (Fig. 6(a,b,e,f)), having a constant amplitude. From that bend, the flow can be considered as both hydrodynamically and thermally developed. The fluid behaves in the same way in each bend and each straight section. However, at higher Reynolds number (Fig. 6(c,d,g,h)), the amplitude of the oscillations becomes irregular whatever the axial location. Regarding Nu, the amplitude tends to decrease along the channel until a significant jump is observed. The jump is observed earlier as Reynolds number increases. This irregular behavior in wavy channels has already been observed and has been interpreted as chaotic flow [35,13], in this paper it is named as non-periodic flow.

To understand the transition from periodic flow to non-periodic flow, the velocity fields in both cases are studied. Velocity fields and relative tangential velocity vectors at different cross-sections between two bends for Re = 224 and 448 are shown in Figs. 7 and 8. The relative tangential velocity is defined as the tangential velocity divided by the mean fluid velocity. For both Reynolds numbers, at the entrance of a bend, the high velocity zone is close to the inner side of that bend (corresponding to the outer side of the previous bend) and then moves towards the outer side due to centrifugal effects (Fig. 7(a) and Fig. 8(a)). In cross-section (b), the relative tangential velocity vectors are mainly towards the inner side of the bend under the effect of centrifugal forces created by the previous bend. For the following cross-sections (c–h), Dean vortices appear, and the number of vortices varies from two to four. Their intensity becomes stronger in the bend and decreases along the straight channel. The direction of the relative tangential velocity changes and shifts towards the inner side of the next bend as shown in cross-section (i). However, it has to be underlined that in cross-section (h), for Re = 224 (Fig. 7), the tangential movement has almost vanished while the Dean vortices are still perceptible for Re = 448 (Fig. 8). By comparing the cross-section (b) and (i), the relative tangential velocity field is almost the same at the entrances of the two bends for Re = 224 (Fig. 7). The only change is the direction, suggesting the flow behavior in the next bend returns to that of the previous bend. For Re = 448, the flow behavior in the coming bend does not return to that of the previous bend, as the instability created in this bend is still significant (Fig. 8). This flow regime is more irregular

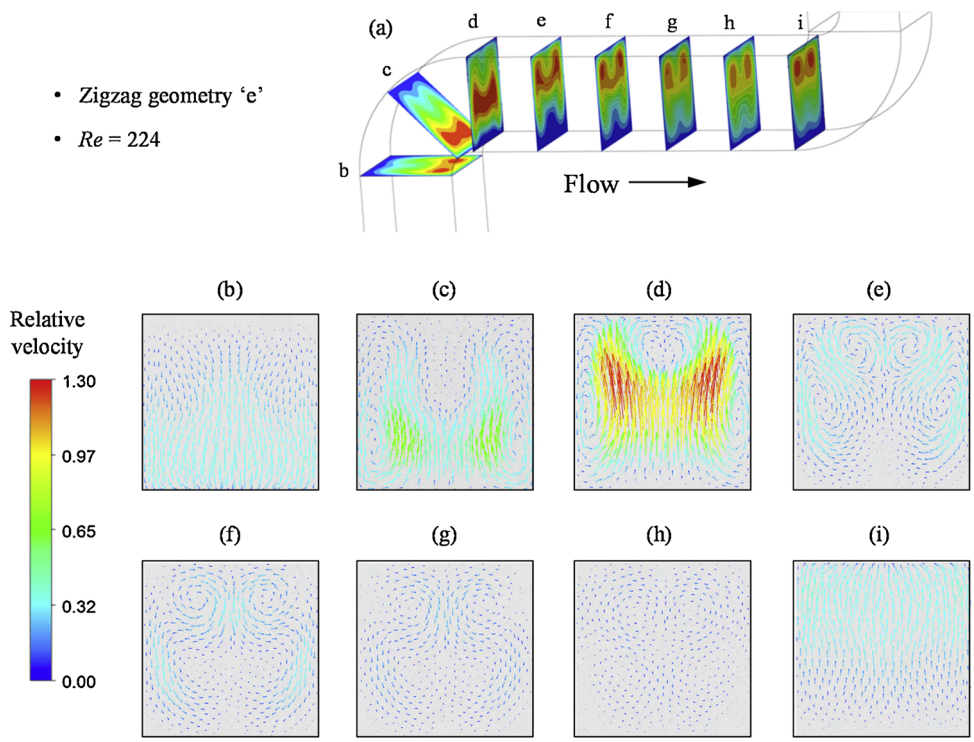

Fig. 7. (a) Velocity fields and (b–i) relative tangential velocity vectors at different cross-sections between two bends at $Re = 224$ in zigzag channel 'e'. The top side in (b–i) corresponds to the outer side of the bend studied.

and unstable, different from that at a Reynolds number of 224 where the fluid spends more time in the straight section.

3.3.3. *Evolution of Nu and f versus L_s*

Different zigzag channels with straight section lengths ranging from 3.5 mm to 12 mm are studied at $Re = 224$. The local Nusselt number Nu and friction factor f from the channel entrance to the exit of the last unit of the zigzag channel are shown in Fig. 9(a–j). The local Nusselt number and friction factor in a straight channel with the same cross-section at the same Reynolds number are also presented as a reference. It is observed that the transition between periodic flow (Fig. 9(d–e, i–j)) and non-periodic flow (Fig. 9(a–c, f–h)) occurs as the straight section

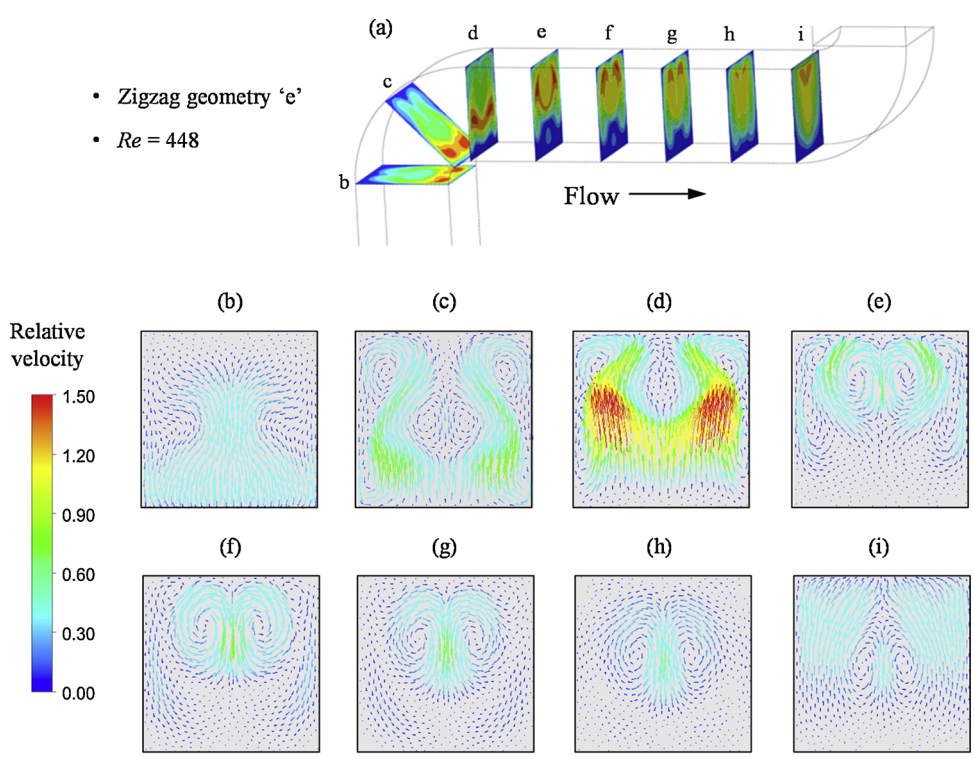

Fig. 8. (a) Velocity fields and (b–i) relative tangential velocity vectors at different cross-sections between two bends at $Re = 448$ in zigzag channel 'e'. The top side in (b–i) corresponds to the outer side of the bend studied.

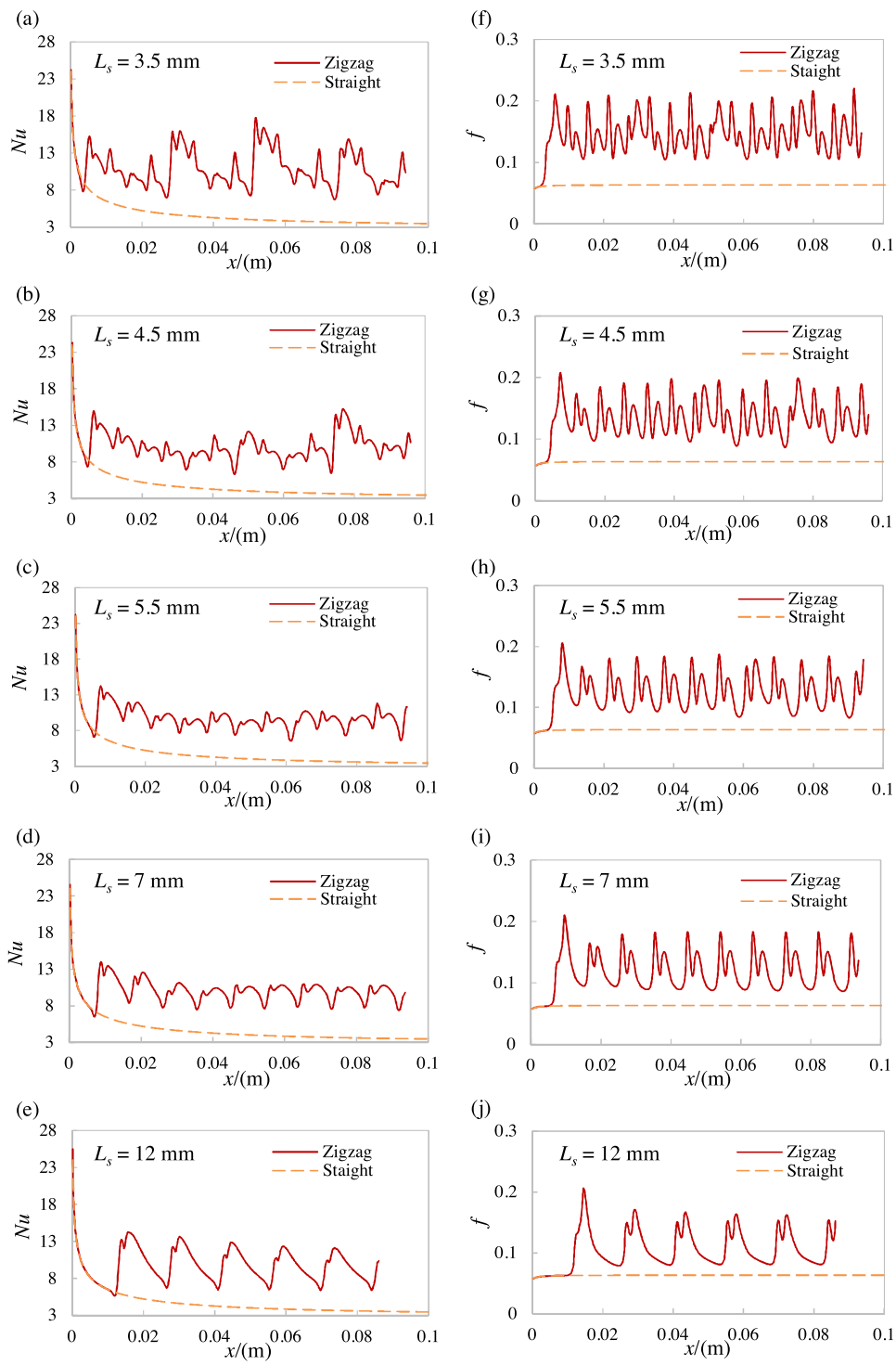

Fig. 9. (a–e) Local Nusselt number and (f–j) Fanning friction factor profiles in the straight channel and the zigzag channel with L_s = 3.5–12 mm at Re = 224.

length is decreased. By analogy with part 3.3.2, where the non-periodic flow occurs by increasing the fluid velocity, it is confirmed that reducing the residence time between two bends favours the occurrence of a non-periodic flow regime.

3.3.4. Fourier analysis for non-periodic flow detection

A fast Fourier analysis was used to analyze the local Nusselt number and the friction factor in the zigzag channels. It converts the signal of Nusselt number and friction factor from the spatial domain to the frequency domain. The fast Fourier transform analysis is applied to ($Nu - Nu_m(L)$) and ($f - f_m(L)$). $Nu_m(L)$ and $f_m(L)$ represent the global Nusselt number and friction factor, respectively, calculated by averaging the local values from the channel inlet (x = 0) to the outlet (x = L). Here two cases are presented with the straight section length L_s equal to 7 mm and 3.5 mm at Re = 224 as shown in Fig. 10. For zigzag channels 'e' with L_s = 7 mm, the Fourier transform spectrum of Nusselt number contains a unique primary frequency f_1 and its harmonic frequencies $2f_1$, $3f_1$, $4f_1$, etc. (Fig. 10(a)). f_1 is equal to the frequency of the bend in the channel given by:

$$f_1 = \frac{\bar{u}}{L_s + L_c} \tag{16}$$

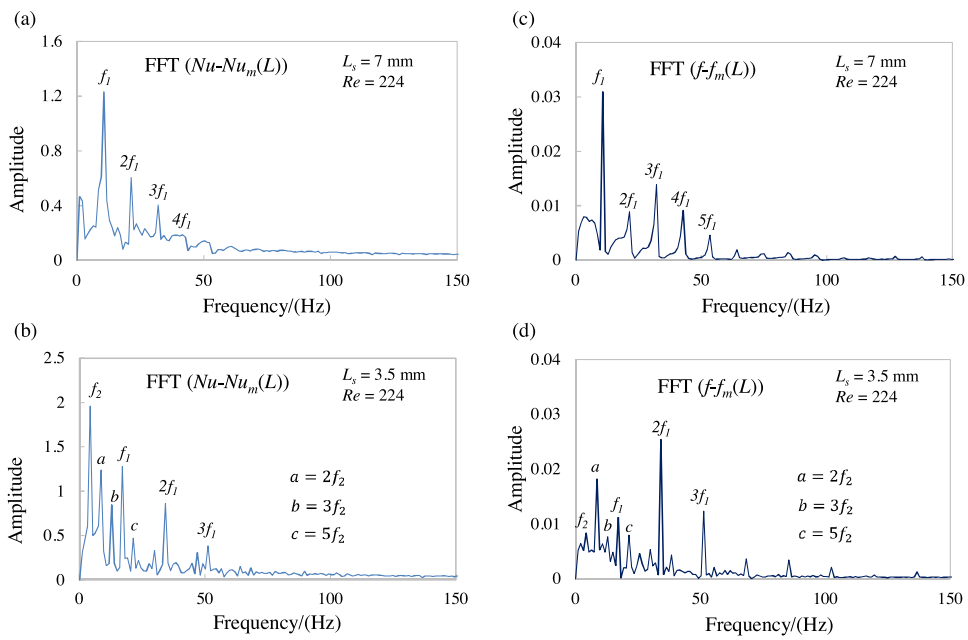

Fig. 10. Fast Fourier transform analysis for Nusselt number and friction factor in zigzag channels with straight section lengths of (a,c) 7 mm and (b,d) 3.5 mm at $Re = 224$.

The same observation can be made in the spectrum of the friction factor where the basic frequency is the same (Fig. 10(b)). These results show that the flow is in a periodic regime with a single oscillation frequency. For zigzag channels 'b' with $L_s = 3.5$ mm (Fig. 10(b,d)), another basic frequency f_2 appears in addition to the primary frequency f_1 in the spectrums of Nusselt number and friction factor. The ratio f_2/f_1 is a quarter. All the other spectral peaks are the harmonic frequencies of these two basic frequencies f_1 and f_2. The flow is no longer in the periodic regime but non-periodic. This analysis methodology has been widely used for flow transition scenario studies although classically it is applied to velocity, not to Nusselt number or friction factor [28–32].

With the help of fast Fourier transform analysis, the flow pattern periodic or non-periodic for different channel configurations at different Reynolds numbers can be distinguished. A map is plotted to show the flow regime as a function of Reynolds number and normalized straight section length L_s/d_h (Fig. 11). For the data marked with a full triangle in the figure, the simulation converged but the grid independence was not achieved. A transient solver has been tested to simulate the condition where $Re = 560$ and $L_s = 3.5$ mm as transient laminar flow was observed in analogous geometries [36]. In the present case, the transient simulations converge towards a steady solution but the converged solution still depends on the mesh grid size. Reducing the mesh size is impractical. In the map, a boundary line between periodic and non-periodic flow can be observed. As mentioned before, the non-periodic flow regime can be achieved by decreasing the straight section length between two bends or by increasing the fluid velocity.

3.4. Global results

3.4.1. Average Nusselt number and friction factor

The average Nusselt number Nu_m and friction factor f_m in the different zigzag channels at different Reynolds numbers were also studied. Two cases of average Nusselt number at $Re = 224$ are presented in Fig. 12: one is in the steady periodic regime with a straight section length of 12 mm, whilst the other is in the non-periodic regime with a straight section length of 3.5 mm. The average Nusselt number in the straight channel is also presented. In both regimes, it can be seen that the Nusselt number quickly becomes stable while, in the straight channel, it decreases along the simulated length. The average Nusselt number stabilizes after several bends, indicating the thermal boundary layer has been fully-developed for both flow regimes within a zigzag channel length of few centimeters.

The average Nusselt number and friction factor at axial coordinate $x = 0.086$ m (channel length of geometry 'g') was chosen as a representation of the global average Nusselt number and friction factor for all the zigzag channels studied, where the thermal boundary layer is considered as fully−developed (denoted by an infinity superscript). The Nusselt number and friction factor are plotted as a function of L_s/d_h, as presented in Fig. 13. In Fig. 13 (a), the Nusselt number increases with increasing Reynolds number for all the channel geometries. Its variation for different L_s/d_h seems to be random at the same Reynolds number, indicating the influence of the straight section length on the heat transfer is not obvious in the zigzag channel. The friction factor decreases with increasing L_s/d_h or Reynolds number, as shown in Fig. 13 (b).

3.4.2. Validation of the simulation results by experiments

An experimental setup, presented in Fig. 14, is used to study heat transfer in a prototype millimetric heat-exchanger which consists of

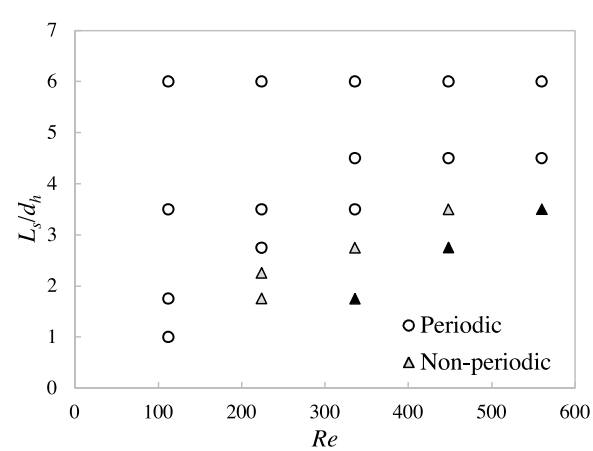

Fig. 11. Map of periodic flow and non-periodic flow in the zigzag channels studied for $Re = .112–560$.

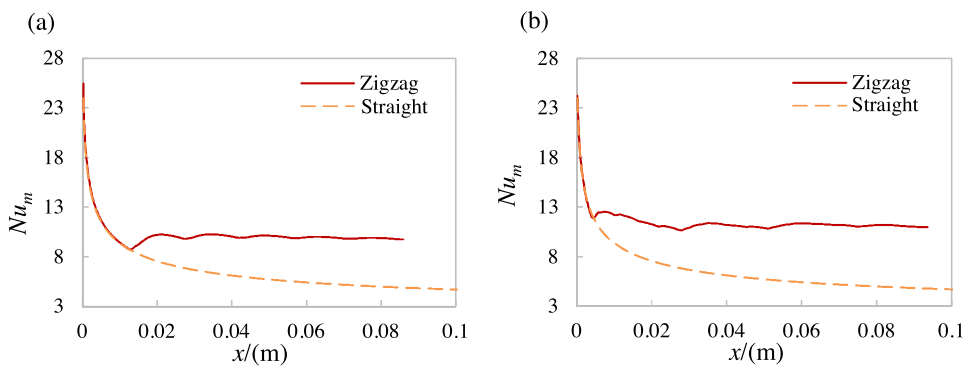

Fig. 12. Average Nusselt number in straight channel and zigzag channel at Re = 224: (a) L_s = 12 mm; (b) L_s = 3.5 mm.

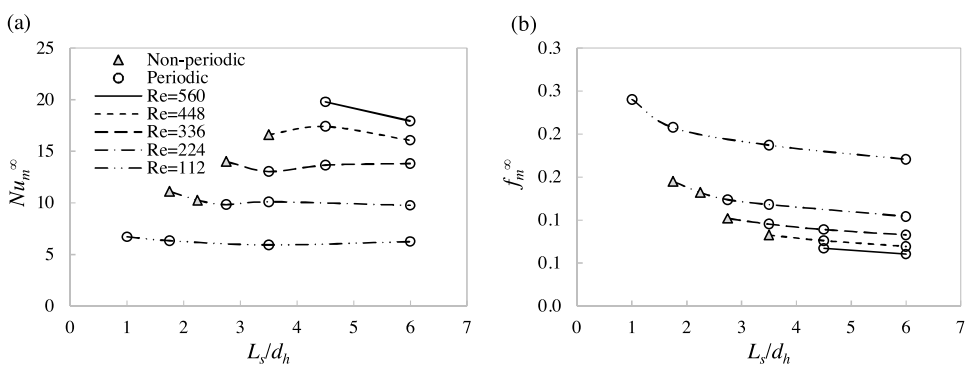

Fig. 13. Fully-developed average Nusselt number (a) and friction factor (b) in the zigzag channels.

three plates: a plate made of aluminum sandwiched between a 'process' plate and a 'utility' plate. The three plates are assembled together using double-sided adhesives cut to fit the channel designs. The aluminum plate is very thin (e_{Al} = 1 mm thickness) and presents a high thermal conductivity (λ_{Al} = 237 W m^{-1} K^{-1}) so that its thermal resistance is very low (e_{Al}/λ_{Al} = 4.2×10^{-6} m^2 K W^{-1}) compared to the maximal global thermal resistance 1/U = 2.5×10^{-4} m^2 K W^{-1} measured in the experiments. The 'process' plate and the 'utility' plate, of 10 mm thickness, are made of PolyMethylMethAcrylate (PMMA), its thermal conductivity is very low to limit the thermal losses (λ_{PMMA} = 0.19 W m^{-1} K^{-1}). In the 'process' plate, a zigzag channel is etched whose geometric parameters are the same as the geometry 'e' simulated, with just a different total length (0.6 m in the experiment compared with 0.1 m in the simulation). In the 'utility' plate, a straight channel with a rectangular cross-section (12 mm width, 6 mm depth) is etched so that it largely covers the zigzag channel in the 'process' plate both in the flow direction and radial direction. The two channels in the two plates (zigzag channel in 'process' plate, straight channel in 'utility' plate) are face to face and at

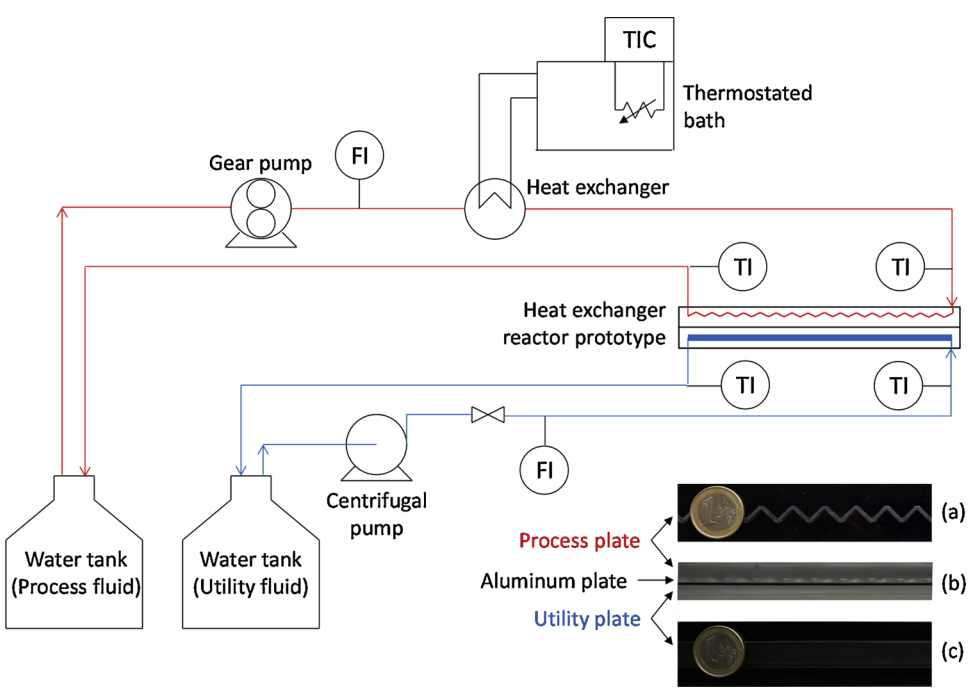

Fig. 14. Experimental setup for the determination of the heat transfer coefficient of wavy millimetric channels. The heat exchanger reactor prototype is composed of a PMMA 'process' plate where the millimetric zigzag channel is etched (top view in (a)), a PMMA 'utility' plate where a larger rectangular straight channel is etched (front view in (c)), both separated by an aluminum plate (side view in (b)).

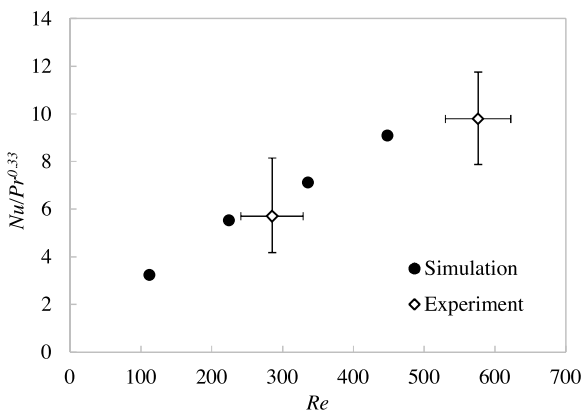

Fig. 15. Comparison of Nu/ $Pr^{0.33}$ from simulation and experiment for the zigzag channel 'e'. The experimental error is estimated from the accuracy of the sensors (± 0.2 kg h^{-1} for the process fluid flowrate, ± 3 kg h^{-1} for the utility fluid flowrate, ± 0.3 °C for the temperatures).

the middle of each plate.

In the experiments, hot water at about 60 °C is introduced in the 'process' plate. It is cooled by cold water at ambient temperature in the 'utility' plate, with a volumetric flowrate of 300 L.h^{-1}. The two fluids flow co-currently. The inlet and outlet temperatures of the two fluids are measured. In order to decrease the thermal loss, the exchanger is surrounded by insulation foam. The process fluid is taken into account for the calculation of heat transfer coefficient as it has larger temperature difference. From the temperature difference (ΔT_p) in process fluid, the heat exchange flux between the two fluids (q) can be calculated using Eq. (17). The thermal losses (q_l) have been previously estimated by introducing just the process fluid (Eq. (17) with $q = 0$), with no flow in the utility plate.

$$q = \dot{m}_p C_{P,p}\, \Delta T_p - q_l \tag{17}$$

where $\dot{m}_p$ is the mass flow rate and $C_{P,p}$ is the specific heat of the process fluid. The global heat transfer coefficient (U) of the mock-up can be calculated by:

$$U = \frac{q}{A_H\, \Delta T_{ml}} \tag{18}$$

where ΔT_{ml} is the logarithmic mean temperature difference. For the sandwiched mock-up, the overall conductance is:

$$\frac{1}{UA_H} = \frac{1}{h_p A_{H,p}} + \frac{e_{Al}}{\lambda_{Al} A_H} + \frac{1}{h_u A_{H,u}} \tag{19}$$

where h_p and h_u are the convection heat transfer coefficient of the process fluid and utility fluid, $A_{H,p}$, $A_{H,u}$ are the heat transfer areas in 'process' plate and 'utility' plate, respectively. In this work, A_H is considered equal to $A_{H,p}$. The heat transfer coefficient h_u of utility fluid (Re > 10^4 during the experiment) can be deduced from the correlation

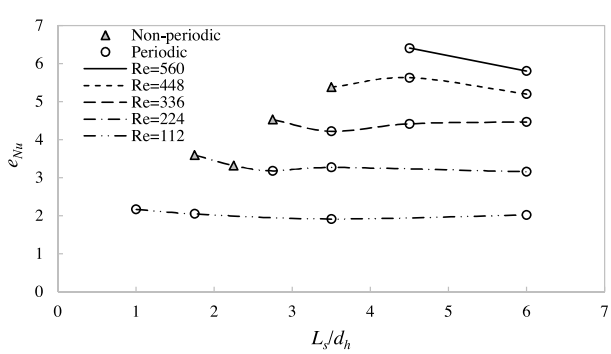

Fig. 16. Heat transfer enhancement in the zigzag channels studied.

of Nusselt proposed by Gnielinski [37]:

$$Nu_u = \frac{h_u d_{h,u}}{\lambda_u} = 0.012\,(Re_u^{0.87} - 280)\, Pr_u^{0.4}\, [1 + (\frac{d_{hu}}{L_u})^{\frac{2}{3}}]\, (\frac{Pr_u}{Pr_w})^{0.11} \tag{20}$$

Pr_u is close to 4 in the experiments. Assuming the wall is at the temperature of the process fluid, Pr_w is estimated to be around 6. Therefore, it can be reasonably assumed that $\left(\frac{Pr_u}{Pr_w}\right)^{0.11} = 1$. The heat transfer coefficient of the process fluid h_p then can be calculated from Eq. (19). The Nusselt number Nu_p can be furtherly obtained by:

$$Nu_p = \frac{h_p d_{h,p}}{\lambda_p} \tag{21}$$

The experimental and simulation results of the geometry 'e' are shown in Fig. 15 where $Nu/Pr^{0.33}$ is plotted as a function of Re as the Pr in the simulation and experiment is different. The power factor of Pr is 0.33 as suggested by Sieder and Tate correlation in laminar flow or Colburn correlation in turbulent flow [38]. It is observed that the simulation results fit well with the experimental data.

3.4.3. Heat transfer enhancement

As discussed above, the zigzag channel configuration enhances heat transfer compared with the straight channel with the same cross-section. This heat transfer enhancement is accompanied by higher pressure drop which has been noted. The heat transfer enhancement factor is defined as:

$$e_{Nu} = \frac{Nu_m{}^{\infty}}{Nu_0{}^{\infty}} \tag{22}$$

where $Nu_0{}^{\infty}$ is the Nusselt number in a straight channel. As mentioned before, for hydraulically and thermally developed laminar flow, $Nu_0{}^{\infty} = 3.091$ for a square channel with H2 thermal boundary condition [34]. e_{Nu} for the studied zigzag configurations at different Reynolds numbers is plotted in Fig. 16. It is observed that the presence of the bends improves the heat transfer significantly, notably at high fluid velocity. e_{Nu} increases with increasing Reynolds number for the different zigzag configurations. Its variation is random in terms of L_s/d_h, indicating the impact of non-periodic flow on heat transfer enhancement is not obvious. Here the pressure drop penalty is not taken into account.

3.4.4. Thermo-hydraulic performance factor

Webb and Eckert have proposed a different way to compare the relative performance of heat exchangers with rough surface tubes compared with heat exchangers with smooth surface tubes [39]. They proposed a list of parameters of interest depending on user constraints (for instance the ratio of the surface areas while constant flow friction power and volumetric flowrate are imposed). By analogy, in the present study, each zigzag channel is compared with a straight channel of the same cross-section assuming that:

- both configurations must provide the same heat exchange capacity in order to heat or cool a fluid from a fixed temperature to a desired one (Eq. (23));
- the fluid flowrate is imposed (Eq. (24)).

$$h_m{}^{\infty} A_H = h_0{}^{\infty} A_{H,0} \tag{23}$$

$$Q = Q_0 \tag{24}$$

Therefore, from Eqs. (1) and (2), the performance factor can be expressed as follows:

$$PF = \frac{\Delta p_0}{\Delta p} \tag{25}$$

In other words, the performance factor considered in the present study compares the pressure drop in a straight channel with that in a zigzag channel with the same cross-section and flow rate. In order to

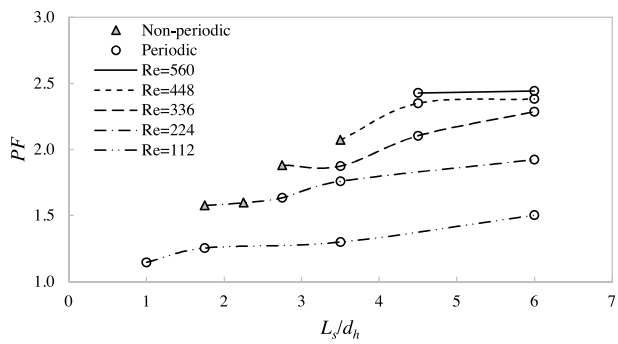

Fig. 17. Thermo-hydraulic performance factor in the zigzag channels studied.

obtain the same heat exchange capacity, the length of both channels will be different. The pressure drop can be expressed as a function of the mean fluid velocity, the Fanning friction factor, the hydraulic diameter and the channel length:

$$\Delta p = 2\rho \bar{u}^2 f^{\infty} \frac{L}{d_h} \tag{26}$$

For same flowrate and hydraulic diameter, the performance factor simplifies to:

$$PF = \frac{f_0^{\infty} L_0}{f^{\infty} L} \tag{27}$$

where L_O is the straight channel length and f_0^{∞} the Fanning friction factor for fully-developed laminar flow in square straight channel [32]:

$$f_0^{\infty} = \frac{14.227}{Re} \tag{28}$$

Considering the same cross-section in the zigzag and straight channels, the ratio of channel lengths is equal to the ratio of heat exchange areas. From Eq. (23), the following expression is then obtained:

$$\frac{L_0}{L} = \frac{A_{\mathrm{H},0}}{A_H} = \frac{h_m{}^{\infty}}{h_0{}^{\infty}} = \frac{Nu_m{}^{\infty}}{Nu_0{}^{\infty}} \tag{29}$$

From Eqs. (27)–(29), the performance factor can finally be expressed as follows:

$$PF = \frac{14.227}{Re} \frac{Nu_m{}^{\infty}}{f^{\infty} Nu_0{}^{\infty}} \tag{30}$$

PF for the channel configurations studied at different Reynolds numbers is presented in Fig. 17. For all the cases studied, *PF* is greater than one, suggesting that the bends significantly enhance the thermo-hydraulic performances of the channel. That means the zigzag channel brings less significant pressure drop compared with the heat transfer enhancement. *PF* increases with increasing Reynolds number or L_s/d_h. The increase with Reynolds number is particularly important at low *Re*. From $Re = 336$, the increase becomes moderate with increasing Reynolds number. Concerning the impact of the straight section, decreasing its length to reach non-periodic flow regime is not interesting in terms of thermo-hydraulic performances in the cases studied. Finally, it has to be noted that by increasing L_s/d_h, the zigzag design will get closer to the straight channel. Therefore, the different curves should converge towards $PF = 1$ for very high L_s/d_h, depicting a bell-shaped curve with an optimal range of L_s/d_h values depending on *Re*. The observed plateaus for $Re = 448$ and $Re = 560$ may suggest that this optimum is between $L_s/d_h = 4.5$ and 6 for these conditions.

4. Conclusions

A numerical method based on the use of the software ANSYS CFX has been developed to study the flow and heat transfer in millimetric zigzag channels with square cross-section and 2 mm hydraulic diameter. The simulations are carried out for the steady laminar flow regime with Reynolds numbers ranging from 112 to 560 and a Prandtl number of 6.13. The channel geometry in terms of straight section length between two bends from 2 mm to 12 mm has been investigated. The flow and heat transfer in a straight channel with the same cross-section is also studied as a reference. The numerical method is validated by comparing with experimental data for Nusselt number obtained in a heat transfer experiment.

The results show that local Nusselt numbers and Fanning friction factors vary along the zigzag channels according to oscillating curves. The amplitude of the oscillations is constant with periodic flow but varies in the case of non-periodic flow. Based on Fourier analysis, a map has been provided which allows to distinguish the conditions in terms of Reynolds number and straight section length that gives a periodic flow or a non-periodic flow. Non-periodic flow is obtained by increasing the fluid velocity or by decreasing the straight section length. For $Re = 560$ and $L_s/d_h = 3.5$, the flow instability created by the bends was too great for steady laminar flow to develop. The heat transfer enhancement and thermo-hydraulic performance factor are quantitatively discussed, which show that the zigzag channel enhances the heat transfer strongly and increases relatively less significantly the pressure drop compared with the straight channel. It appeared that non-periodic flow is not particularly interesting in terms of thermo-hydraulic performances. All these data should be very useful for the design of high-performance heat exchangers-reactors. The impact of other geometric parameters, such as the hydraulic diameter, the curvature radius of the bends and their angle should be studied to complete this work.

Acknowledgment

This work was performed using HPC resources from CALMIP.

References

[1] Z. Anxionnaz, M. Cabassud, C. Gourdon, P. Tochon, Heat exchanger/reactors (HEX reactors): concepts, technologies: state-of-the-art, Chem. Eng. Process. Process Intensif. 47 (2008) 2029–2050, https://doi.org/10.1016/j.cep.2008.06.012.
[2] Z. Anxionnaz-Minvielle, M. Cabassud, C. Gourdon, P. Tochon, Influence of the meandering channel geometry on the thermo-hydraulic performances of an intensified heat exchanger/reactor, Chem. Eng. Process. Process Intensif. 73 (2013) 67–80, https://doi.org/10.1016/j.cep.2013.06.012.
[3] R.M. Manglik, J. Zhang, A. Muley, Low Reynolds number forced convection in three-dimensional wavy-plate-fin compact channels: fin density effects, Int. J. Heat Mass Transf. 48 (2005) 1439–1449, https://doi.org/10.1016/j.ijheatmasstransfer.2004.10.022.
[4] L. Wang, F. Liu, Forced convection in slightly curved microchannels, Int. J. Heat Mass Transf. 50 (2007) 881–896, https://doi.org/10.1016/j.ijheatmasstransfer.2006.08.016.
[5] Y. Sui, C.J. Teo, P.S. Lee, Y.T. Chew, C. Shu, Fluid flow and heat transfer in wavy microchannels, Int. J. Heat Mass Transf. 53 (2010) 2760–2772, https://doi.org/10.1016/j.ijheatmasstransfer.2010.02.022.
[6] Y. Sui, P.S. Lee, C.J. Teo, An experimental study of flow friction and heat transfer in wavy microchannels with rectangular cross section, Int. J. Therm. Sci. 50 (2011) 2473–2482, https://doi.org/10.1016/j.ijthermalsci.2011.06.017.
[7] N.R. Rosaguti, D.F. Fletcher, B.S. Haynes, Laminar flow and heat transfer in a periodic serpentine channel with semi-circular cross-section, Int. J. Heat Mass Transf. 49 (2006) 2912–2923, https://doi.org/10.1016/j.ijheatmasstransfer.2006.02.015.
[8] R. Gupta, P.E. Geyer, D.F. Fletcher, B.S. Haynes, Thermohydraulic performance of a periodic trapezoidal channel with a triangular cross-section, Int. J. Heat Mass Transf. 51 (2008) 2925–2929, https://doi.org/10.1016/j.ijheatmasstransfer.2007.09.017.
[9] N.R. Rosaguti, D.F. Fletcher, B.S. Haynes, Laminar flow and heat transfer in a periodic serpentine channel, Chem. Eng. Technol. 28 (2005) 353–361, https://doi.org/10.1002/ceat.200407148.
[10] P.E. Geyer, N.R. Rosaguti, D.F. Fletcher, B.S. Haynes, Thermohydraulics of square-section microchannels following a serpentine path, Microfluid. Nanofluidics 2 (2006) 195–204, https://doi.org/10.1007/s10404-005-0062-7.
[11] P.E. Geyer, D.F. Fletcher, B.S. Haynes, Laminar flow and heat transfer in a periodic trapezoidal channel with semi-circular cross-section, Int. J. Heat Mass Transf. 50 (2007) 3471–3480, https://doi.org/10.1016/j.ijheatmasstransfer.2007.01.050.
[12] N.R. Rosaguti, D.F. Fletcher, B.S. Haynes, Low-Reynolds number heat transfer enhancement in sinusoidal channels, Chem. Eng. Sci. 62 (2007) 694–702, https://doi.org/10.1016/j.ces.2006.09.045.
[13] Z. Zheng, D.F. Fletcher, B.S. Haynes, Chaotic advection in steady laminar heat

transfer simulations: periodic zigzag channels with square cross-sections, Int. J. Heat Mass Transf. 57 (2013) 274–284, https://doi.org/10.1016/j.ijheatmasstransfer.2013.12.056.
[14] H. Aref, Stirring by chaotic advection, J. Fluid Mech. 143 (1984) 1, https://doi.org/10.1017/S0022112084001233.
[15] R.H. Liu, M.A. Stremler, K.V. Sharp, M.G. Olsen, J.G. Santiago, R.J. Adrian, H. Aref, D.J. Beebe, Passive mixing in a three-dimensional serpentine microchannel, J. Microelectromech. Syst. 9 (2000) 190–197.
[16] A.D. Stroock, S.K. Dertinger, A. Ajdari, I. Mezić, H.A. Stone, G.M. Whitesides, Chaotic mixer for microchannels, Science 295 (2002) 647–651.
[17] J. Aubin, D.F. Fletcher, J. Bertrand, C. Xuereb, Characterization of the mixing quality in Micromixers, Chem. Eng. Technol. 26 (2003) 1262–1270, https://doi.org/10.1002/ceat.200301848.
[18] F. Jiang, K.S. Drese, S. Hardt, M. Küpper, F. Schönfeld, Helical flows and chaotic mixing in curved micro channels, AIChE J. 50 (2004) 2297–2305, https://doi.org/10.1002/aic.10188.
[19] V. Kumar, K.D.P. Nigam, Laminar convective heat transfer in chaotic configuration, Int. J. Heat Mass Transf. 50 (2007) 2469–2479, https://doi.org/10.1016/j.ijheatmasstransfer.2006.12.029.
[20] C. Castelain, A. Mokrani, Y. Le Guer, H. Peerhossaini, Experimental study of chaotic advection regime in a twisted duct flow, Eur. J. Mech. BFluids. 20 (2001) 205–232, https://doi.org/10.1016/S0997-7546(00)01116-X.
[21] H. Peerhossaini, C. Castelain, Y. Le Guer, Heat exchanger design based on chaotic advection, Exp. Therm. Fluid Sci. 7 (1993) 333–344, https://doi.org/10.1016/0894-1777(93)90056-O.
[22] N. Acharya, M. Sen, C. Hsueh-Chia, Heat transfer enhancement in coiled tubes by chaotic mixing, Int. J. Heat Mass Transf. 35 (1992) 2475–2489, https://doi.org/10.1016/0017-9310(92)90090-F.
[23] Z. Zheng, A.M. Johnston, D.F. Fletcher, B.S. Haynes, Heat exchanger specification: coupling design and surface performance evaluation, Chem. Eng. Res. Des. 93 (2015) 392–401, https://doi.org/10.1016/j.cherd.2014.04.015.
[24] S. Pati, S.K. Mehta, A. Borah, Numerical investigation of thermo-hydraulic transport characteristics in wavy channels: comparison between raccoon and serpentine channels, Int. Commun. Heat Mass Transf. 88 (2017) 171–176, https://doi.org/10.1016/j.icheatmasstransfer.2017.09.001.
[25] S. Elgue, A. Conté, C. Gourdon, Y. Bastard, Direct fluorination of 1,3-dicarbonyl compound in a continuous flow reactor at industrial scale, Chem. Today 30 (2012).
[26] L. Despènes, S. Elgue, C. Gourdon, M. Cabassud, Impact of the material on the thermal behaviour of heat exchangers-reactors, Chem. Eng. Process. Process Intensif. 52 (2012) 102–111, https://doi.org/10.1016/j.cep.2011.11.005.
[27] N. Di Miceli Raimondi, N. Olivier-Maget, N. Gabas, M. Cabassud, C. Gourdon, Safety enhancement by transposition of the nitration of toluene from semi-batch reactor to continuous intensified heat exchanger reactor, Chem. Eng. Res. Des. 94 (2015) 182–193, https://doi.org/10.1016/j.cherd.2014.07.029.
[28] G.E. Karniadakis, G.S. Triantafyllou, Three-dimensional dynamics and transition to turbulence in the wake of bluff objects, J. Fluid Mech. 238 (1992) 1–30, https://doi.org/10.1017/S0022112092001617.
[29] A.M. Guzmán, C.H. Amon, Dynamical flow characterization of transitional and chaotic regimes in converging–diverging channels, J. Fluid Mech. 321 (1996) 25, https://doi.org/10.1017/S002211209600763X.
[30] A.M. Guzmán, M. Del Valle, Heat transfer enhancement in grooved channels due to flow bifurcations, Heat Mass TransferWaerme- Stoffuebertragung. 42 (2006) 967–975, https://doi.org/10.1007/s00231-005-0065-7.
[31] J. Zhang, N.S. Liu, X.Y. Lu, Route to a chaotic state in fluid flow past an inclined flat plate, Phys. Rev. E - Stat. Nonlinear Soft Matter Phys. 79 (2009) 1–4, https://doi.org/10.1103/PhysRevE.79.045306.
[32] Y. Sui, C.J. Teo, P.S. Lee, Direct numerical simulation of fluid flow and heat transfer in periodic wavy channels with rectangular cross-sections, Int. J. Heat Mass Transf. 55 (2012) 73–88, https://doi.org/10.1016/j.ijheatmasstransfer.2011.08.041.
[33] R.K. Shah, A.L. London, Laminar Flow Forced Convection in Ducts: A Source Book for Compact Heat Exchanger Analytical Data, Academic Press, Inc, New York, 1978.
[34] R.K. Shah, Laminar flow friction and forced convection heat transfer in ducts of arbitrary geometry, Int. J. Heat Mass Transf. 18 (1975) 849–862.
[35] H.M. Xia, Z.P. Wang, S.Y.M. Wan, F.F. Yin, Numerical study on microstructured reactor with chaotic heat and mass transfer and its potential application for exothermic process, Chem. Eng. Res. Des. 90 (2012) 1719–1726, https://doi.org/10.1016/j.cherd.2012.03.019.
[36] Z. Zheng, D.F. Fletcher, B.S. Haynes, Transient laminar heat transfer simulations in periodic zigzag channels, Int. J. Heat Mass Transf. 71 (2014) 758–768, https://doi.org/10.1016/j.ijheatmasstransfer.2013.12.056.
[37] V. Gnielinski, New equations for heat and mass transfer in turbulent pipe and channel flow, Int Chem Eng. 16 (1976) 359–368.
[38] F.P. Incropera, A.S. Lavine, T.L. Bergman, D.P. DeWitt, Fundamentals of Heat and Mass Transfer, Wiley, 2007.
[39] R.L. Webb, E.R.G. Eckert, Application of rough surfaces to heat exchanger design, Int. J. Heat Mass Transf. 15 (n.d.) 1647–1658.